Precise Localization of an Indoor Robot using Robotic Total Station and Error State Extended Kalman Filter

Sahar ABOLHASANI, Li ZHANG, Volker SCHWIEGER, Germany

Key words: Robotic Total Station, Error State Extended Kalman Filter

SUMMARY

Through the digitalization of the construction sector, more and more robots are being used on the construction site. The construction site is normally unstructured, and the positioning of the robot (incl. position, velocity, and orientation) is essential (e.g., for safety). In the context of existing buildings, construction sites are typically indoor, and the Robotic Total Station (RTS) can be used for precise localization of the robots. However, the RTS could not measure when the Line of Sight (LoS) to the target is lost. In this paper, the methods of integrating the RTS, odometer and IMU data using the Error State Extended Kalman Filter (ES-EKF) were introduced. The ES-EKF is running in real-time on an indoor robot; measurements were carried out to evaluate the accuracy and also the robustness of the ES-EKF in the absence of RTS and odometer data.

The position difference between the ES-EKF and the laser tracker is about 0.31cm and the standard deviation of the difference is 0.3cm. In our test, the results of the ES-EKF will drift immediately if neither the RTS nor the odometer data is available. If only the RTS measurement, e.g. in case of losing the LoS, is not available, the odometer could still be used to correct the drift of the IMU for a short time.

Precise Localization of an Indoor Robot using Robotic Total Station and Error State Extended Kalman Filter

Sahar ABOLHASANI, Li ZHANG, Volker SCHWIEGER, Germany

1. INTRODUCTION

The worker shortage in the construction sector keeps increasing. In 2021, 33.5 % of German building construction companies and 37.9 % of German civil engineering companies had difficulties hiring new workers IFO (2021). In 2022, the U.S. registered a shortage of 430,000 construction-industry workers Katara (2022). Nevertheless, the construction sector remains one of the least digitized sectors worldwide Barbosa et al. (2017). In this context, the stagnating productivity of the construction sector can be increased through digitization and automation Knippers et al. (2021).

The vision of the Cluster of Excellence Integrative Computational Design and Construction for Architecture (IntCDC) at the University of Stuttgart and the Max Planck Institute for Intelligent Systems is to harness the full potential of digital technologies to automate the whole construction process and reduce human labour. That is realized through “co-designing” methods, processes, and systems based on interdisciplinary research encompassing architecture, structural engineering, building physics, engineering geodesy, manufacturing and systems engineering, computer science and robotics, and humanities and social sciences (IntCDC, 2018).

Recently, advances in technology have enabled more automation in the building process, especially on-site construction (Meyer, 2003). Gassel et al. (2003) used robotic technology for assembling wall panels. Lauer et al. (2023) realized the on-site assembly of timber components for a biomimetic shell, which was successfully completed within the cluster of IntCDC.

Additionally, some efforts have been directed to the interior construction tasks, e.g. finishing tasks of surface structures for ceilings, floors and walls (Warszawski & Navon 1986, Vähä et al. 2013, Brosque et al. 2020). For instance, in Sorour et al. (2011), a roller-based autonomous robot for painting the interior walls of buildings was introduced.

However, in the context of existing buildings, the vision of autonomous robotic systems is still far away, given the unstructured environment and the variety of different scenarios. The further densification of urban structures in the developed world is a central task to meet the enormous demand for inner-city living, minimize the need for additional transport infrastructure, and reduce environmental pollution and land consumption (Knippers et al. 2021). In Germany alone, vertical expansion of the urban building stock could realize an additional 1.5 million housing units, saving the equivalent of up to 250 million square meters of undeveloped land (Tichelmann et al. 2016), which is crucial to the government's goal of halving land consumption by 2030 (BMUB, 2017).

Thus, one research project within IntCDC, in which the Institute of Engineering Geodesy (IIGS) participates, deals with the innovative topic of robotic construction in the interior fitting for the

expansion of an existing building. Therefore, the robots should autonomously navigate through the environment. For this, the localization of the robots is of great importance. Localization or positioning, in this context, refers to the estimation of the position and the orientation of a mobile robot in the motion area in real-time. The high accuracy of positioning is a prerequisite to ensure that the robot can complete the task and ensure the safety of the human–machine environment (Huang et al. 2023). Indoor precise tasks demanding direct contact between the manipulator and building components need 2–3-millimeter accuracy (Shohet & Rosenfeld 1997, Feng et al. 2014). Considering the unstructured environment and obstacles inside the existing buildings, reaching this accuracy is a challenging issue. Although Simultaneous Localization and Mapping (SLAM) algorithms have had significant improvements in the last decade, their long-term operation remains a major challenge, primarily due to the wide spectrum of perturbations robotic systems may encounter (Bujanca et al. 2021). The integration of Global Navigation Satellite Systems (GNSS) with a low-cost Inertial Measurement Unit (IMU) and an odometer is another extensively used solution in this field. Odometer fusion decreases the accumulated drift of IMU positioning in the case of the absence of GNSS signals, which happens in urban areas. In this paper, the infeasibility of GNSS application in the indoor scenario leads to the search for an alternative sensor instead of GNSS. The desired high positioning accuracy suggests the use of a Robotic Total Station (RTS). The only adverse issue related to RTS is the necessity of the Line of Sight (LoS) between the RTS and the target reflector. In this paper, RTS/IMU and odometer sensor fusion is proposed. The odometer measurements mitigate the drift of the IMU in the case of blockages for the LoS of the RTS through obstacles.

Filtering methods are the most common techniques for multi-sensor fusion. Kalman Filter (KF) and its extension for nonlinear models, Extended Kalman Filter (EKF), are optimal recursive data processing algorithms that blend all available information, including measurement outputs, prior knowledge about the system, and measuring sensors, to estimate the state variables in such a manner that the error is statistically minimized (Maybeck, 1997). Madyastha (2011), Guo et al. (2019), Youn & Gadsden (2019), Liu et al. (2019) and Markovic et al. (2022) compared the EKF and the so-called Error State Extended Kalman Filter (ES-EKF). The ES-EKF calculates the states of the robot as well as the bias of the IMU. The error state is generally small in magnitude, which prevents singularities and gimbal lock from occurring (Markovic et al. 2022). The aforementioned previous works on ES-EKF are for outdoor applications, where the GNSS and IMU are integrated.

This paper is organized as follows: Section 2 presents the basis for ES-EKF. Section 3 presents data collection by the robot system and the implemented filter. The results are presented in Section 4 and validated by comparing them to a ground truth. Moreover, the performance of the method in the case of the RTS loss of LoS is investigated. In the last section, the results are discussed, and accordingly, new ideas are suggested to improve the related future work.

2. ERROR STATE EXTENDED KALMAN FILTER

The main concept of the ES-EKF consists of the determination of two parts: nominal state $\boldsymbol{x_n}$ and error state $\boldsymbol{\delta x}$. The true state of the moving object $\boldsymbol{x_t}$ is given as a combination of $\boldsymbol{x_n}$ and $\boldsymbol{\delta x}$.

2.1 Nominal State

The nominal state x_n is propagated using a sensor with high-frequency observations, which is usually an IMU. For a moving object, the nominal state x_n ($\in R^{16}$) can be written as:

$$\boldsymbol{x}_n = \begin{bmatrix} \boldsymbol{p} \\ \boldsymbol{v} \\ \boldsymbol{q} \\ \boldsymbol{a_b} \\ \boldsymbol{\omega_b} \end{bmatrix}, \tag{1}$$

where $\boldsymbol{p} \in R^3$ represents 3D-position, $\boldsymbol{v} \in R^3$ 3D-velocity, and $\boldsymbol{q} \in R^4$ is the orientation of the platform in the form of a quaternion. The vectors $\boldsymbol{a_b} \in R^3$ and $\boldsymbol{\omega_b} \in R^3$ are the biases of acceleration and angular velocity from the IMU. The quaternion will not be introduced. Details can be found in Sola (2017) and Youn & Gadsden (2019). The work presented in Sola (2017) and Youn & Gadsden (2019). gives an overview of quaternion kinematics and provides an intuitive insight into the technique of error state filtering, and serves as a starting point for the approach proposed in this paper. The IMU consists of three-axis accelerometers and three-axis gyroscopes. Their measurements are acceleration $\boldsymbol{a_m}$ and angular velocity $\boldsymbol{\omega_m}$, however, the raw measurements contain the bias, and they should be corrected by reducing the bias. By integrating the acceleration with the time Δt, the velocity and the position change of the platform can be calculated. And by integrating the angular velocity with time Δt, the orientation change can be calculated. With the known initial values of velocity, position, and orientation, the coordinates and attitude of the platform can be evaluated at any time. The explained prediction process can be described by the following kinematic equations:

$$\boldsymbol{p} \leftarrow \boldsymbol{p} + \boldsymbol{v} \cdot \Delta t + \frac{1}{2} \cdot (\boldsymbol{R} \cdot (\boldsymbol{a_m} - \boldsymbol{a_b}) + \boldsymbol{g}) \cdot \Delta t^2, \tag{2}$$

$$\boldsymbol{v} \leftarrow \boldsymbol{v} + (\boldsymbol{R} \cdot (\boldsymbol{a_m} - \boldsymbol{a_b}) + \boldsymbol{g}) \cdot \Delta t, \tag{3}$$

$$\boldsymbol{q} \leftarrow \boldsymbol{q} \otimes \boldsymbol{q}\{(\boldsymbol{\omega_m} - \boldsymbol{\omega_b}) \cdot \Delta t\}, \tag{4}$$

$$\boldsymbol{a_b} \leftarrow \boldsymbol{a_b}, \tag{5}$$

$$\boldsymbol{\omega_b} \leftarrow \boldsymbol{\omega_b}, \tag{6}$$

where $\leftarrow$ means the prediction of the state vector from one epoch to the next epoch, $\otimes$ represents the quaternion product operator, and $\boldsymbol{R}$ is the quaternion to rotation conversion matrix. $\boldsymbol{g}$ contains the gravity in the z-axis.

2.2 Error State

The nominal state $\boldsymbol{x}_n$ does not consider the noise terms and other possible errors. Therefore, the resulting accumulated errors and model inaccuracies are collected in the following error state $\boldsymbol{\delta x}$ ($\in R^{15}$):

$$\boldsymbol{\delta x} = \begin{bmatrix} \boldsymbol{\delta p} \\ \boldsymbol{\delta v} \\ \boldsymbol{\delta \theta} \\ \boldsymbol{\delta a_b} \\ \boldsymbol{\delta \omega_b} \end{bmatrix}. \tag{7}$$

The equations related to the kinematics of the error state can be written as:

$$\boldsymbol{\delta p} \leftarrow \boldsymbol{\delta p} + \boldsymbol{\delta v} \cdot \Delta t, \tag{8}$$

$$\boldsymbol{\delta v} \leftarrow \boldsymbol{\delta v} + (-\boldsymbol{R} \cdot [\boldsymbol{a_m} - \boldsymbol{a_b}]_\times \cdot \boldsymbol{\delta\theta} - \boldsymbol{R} \cdot \boldsymbol{\delta a_b} + \boldsymbol{\delta g}) \cdot \Delta t + \boldsymbol{v_w}, \tag{9}$$

$$\boldsymbol{\delta\theta} \leftarrow \boldsymbol{R^T} \cdot \{(\boldsymbol{\omega_m} - \boldsymbol{\omega_b}) \cdot \Delta t\} \cdot \boldsymbol{\delta\theta} - \boldsymbol{\delta\omega_b} \cdot \Delta t + \boldsymbol{\theta_w}, \tag{10}$$

$$\boldsymbol{\delta a_b} \leftarrow \boldsymbol{\delta a_b} + \boldsymbol{a_{bw}}, \tag{11}$$

$$\boldsymbol{\delta\omega_b} \leftarrow \boldsymbol{\omega_b} + \boldsymbol{\omega_{bw}}, \tag{12}$$

where $\boldsymbol{v_w}$, $\boldsymbol{\theta_w}$, $\boldsymbol{a_{bw}}$ and $\boldsymbol{\omega_{bw}}$ are the disturbances of the velocity, orientation and bias estimates, modelled as white Gaussian noise. The disturbance vector $\boldsymbol{w} = [\boldsymbol{v_w}\ \boldsymbol{\theta_w}\ \boldsymbol{a_{bw}}\ \boldsymbol{\omega_{bw}}]$ is with $E(\boldsymbol{w}) = \boldsymbol{0}$. $\boldsymbol{q}$ and $\boldsymbol{\theta}$ are error states of the quaternion and the orientation, respectively, they can be converted to each other, more details are referred to Sola (2017). The skew-operator or cross-operator $[\cdot]_\times$ produces cross-product matrix. In parallel with the integration of the nominal state, the ES-EKF predicts error state and its covariance matrix $\boldsymbol{P}$:

$$\boldsymbol{\delta x} \leftarrow \boldsymbol{F_x} \cdot \widehat{\boldsymbol{\delta x}} + \boldsymbol{F_w} \cdot \boldsymbol{w}, \tag{13}$$

$$\boldsymbol{P} \leftarrow \boldsymbol{F_x} \cdot \boldsymbol{P} \cdot \boldsymbol{F_x^T} + \boldsymbol{F_w} \cdot \boldsymbol{P_w} \cdot \boldsymbol{F_w^T}, \tag{14}$$

where $\boldsymbol{F_x}$, $\boldsymbol{F_w}$ are the Jacobian of the kinematic equations with respect to the error state $\boldsymbol{\delta x}$ and disturbance $\boldsymbol{w}$ respectively, and $\boldsymbol{P_w}$ is the covariance matrix of the disturbances.

2.3 Observation Models

The filter correction is performed at the arrival of information other than IMU (e.g., GNSS, RTS, odometer, etc.), which generally happens at a much lower rate than the prediction, and they are considered as observations. This correction provides a posterior estimation of the error state. The observations $\boldsymbol{z}$ are described according to:

$$\boldsymbol{z} = \boldsymbol{h}(\boldsymbol{x_t}) + \boldsymbol{v}, \tag{15}$$

where $\boldsymbol{h}$ is a general non-linear function of the system and $\boldsymbol{v}$ is observation error and modelled white Gaussian noise with the covariance matrix $\boldsymbol{V}$:

$$\boldsymbol{K} = \boldsymbol{P} \cdot \boldsymbol{H^T} \cdot (\boldsymbol{H} \cdot \boldsymbol{P} \cdot \boldsymbol{H^T} + \boldsymbol{V})^{-1}, \tag{16}$$

$$\widehat{\boldsymbol{\delta x}} \leftarrow \boldsymbol{K} \cdot (\boldsymbol{z} - \boldsymbol{h}(\boldsymbol{x_t})), \tag{17}$$

$\boldsymbol{K}$ is called as gain matrix, $\boldsymbol{H}$ is the Jacobian matrix of the observations $\boldsymbol{z}$ with respect to the error state $\boldsymbol{\delta x}$. After this, the estimated error state $\widehat{\boldsymbol{\delta x}}$ is injected into the nominal state, then $\widehat{\boldsymbol{\delta x}}$ is reset to zero, and the whole process starts over again with the propagation part:

$$\widehat{\boldsymbol{x_t}} = \boldsymbol{x_n} \oplus \widehat{\boldsymbol{\delta x}}. \tag{18}$$

$$\boldsymbol{P} \leftarrow (\boldsymbol{I} - \boldsymbol{K} \cdot \boldsymbol{H}) \cdot \boldsymbol{P}. \tag{19}$$

The observations in the ES-EKF are from RTS and odometers, therefore two observation models for RTS and odometers will be illustrated in the following sections.

2.3.1 RTS

The original observations of an RTS are:

- horizontal angle Hz: horizontal angle between the zero direction of the RTS and the prism,
- vertical angle V: vertical angle of prism,
- slope distance S: slope distance between the zero point of the RTS and the prism.

The Cartesian coordinates of the prism in the local reference frame (l) can be calculated from these observations using the following equation:

$$\boldsymbol{r}_{RTS} = \begin{bmatrix} x \\ y \\ z \end{bmatrix} = \begin{bmatrix} X_0 + S \cdot \sin V \cdot \cos(Hz + \alpha) \\ Y_0 + S \cdot \sin V \cdot \sin(Hz + \alpha) \\ Z_0 + S \cdot \cos V \end{bmatrix}. \tag{20}$$

The rotation α and three translations (X_0, Y_0, Z_0) are the results from free stationing. Additionally, the velocities of the robot $\boldsymbol{v}^l_{RTS}$ can be calculated from the RTS measurements between two epochs, and they are also used as observations as well. The observation of RTS can be written as:

$$\boldsymbol{z}_{RTS} = \begin{pmatrix} \boldsymbol{r}_{RTS} \\ \boldsymbol{v}_{RTS} \end{pmatrix}, \tag{21}$$

2.3.2 Odometer

The odometer could provide the linear velocity in the movement direction (v_{odo}) and the angular velocity around the z-axis (ω_{odo}). The observation of odometer can be written as:

$$\boldsymbol{z}_{odo} = \begin{pmatrix} v_{odo} \\ \omega_{odo} \end{pmatrix}. \tag{22}$$

More equations of the ES-EKF will not be given in this paper due to limited pages.

3 ROBOT PLATFORM AND COORDINATE TRANSFORMATIONS

3.1 Robot Platform and Sensors

The robot platform Robotnik RB-Vogui-6 (see Figure 1) is equipped with different sensors (e.g., IMU, odometer, cameras, and laser scanners). The IMU and odometer were used for sensor fusion. The robot is equipped with a VN-100 IMU (Vectorav, 2025) consisting of an accelerometer and a gyroscope measuring the acceleration and angular velocity at 200 Hz. The specification of the IMU can be found in Table 1.

Figure 1: Robotnik RB-Vogui-6 with lever arms

Table 1: VN-100 IMU specification (Vectorav, 2025)

accelerometer noise density	$0.14\ mg\sqrt{Hz}$
accelerometer in-run bias stability	$< 0.04\ mg$
gyroscope noise density	$0.0035°/s/\sqrt{Hz}$
gyroscope in-run bias stability	$< 10°/\mathrm{hr}$

The odometers (or wheel encoders) on the robot platform provide the velocity in the movement direction and angular velocity around the z-axis with a sampling rate of 4.5 Hz.

To get a precise absolute position of the robot, the RTS Trimble S7 is used. A prism was mounted on the robot (see Figure 1). The measurements of RTS were taken at 10 Hz. The Trimble S7 has an accuracy of 4mm+ 2ppm for distance measurements. The Finelock positioning precision is 1mm (up to 300 m) in the kinematic mode, and the angle accuracy could be estimated, which is distance-dependent.

Generally, in the Kalman Filter, the process noise ($\boldsymbol{P_w}$ in equation (14), in our case it is from the IMU) and the measurement noise ($\boldsymbol{V}$ in equation (16), in our case it is from the RTS and odometer) are essential. For the initialization of $\boldsymbol{P_w}$ and $\boldsymbol{V}$, the specification for the IMU and RTS was regarded. However, no information was available about the accuracy of odometer measurements; their values were tuned empirically.

The robot platform Robotnik RB-Vogui-6 is equipped with a control system powered by an Intel i7 CPU running the Robot Operating System (ROS, version Melodic) in Ubuntu 18.04. ROS package was developed at IIGS to send the RTS measurement to the robot platform (via Raspberry Pi and TCP/IP protocol), so that all the sensors publish their measurements in ROS, and one ROS node was implemented to run the ES-EKF, so that the localization of the robot is realized in real-time. The Raspberry Pi, which is connected with RTS and used as the control computer of the RTS, uses Network Time Protocol (NTP) to synchronize with a local server, which is also the NTP time server of ROS on the robot. The NTP time server of ROS on the robot is synchronized with the NTP time server of the University of Stuttgart. The intrinsic synchronization between the distance and angle measurement

(within RTS) is up to several milliseconds. Considering the velocity of the robot here is under 0.5m/s, the intrinsic synchronization within the RTS is negligible when considering the instrument accuracy in the range of 1-3 mm for kinematic applications.

3.2 Coordinate Systems and Transformations

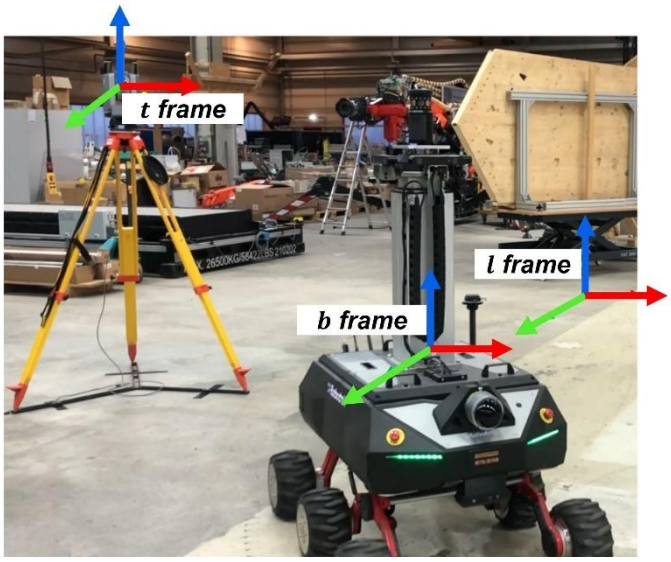

Figure 2: Coordinate Systems

Different coordinate systems are defined (see Figure 2):

- local reference frame (l): a predefined right-handed 3D local reference, and the z-axis is aligned with the local gravity vector. Its origin could be defined arbitrarily.
- RTS frame (t): this coordinate system has the origin at the instrument zero point. The z-axis coincides with the local gravity vector. The x-axis points towards the zero point of the horizontal angle sensor within the RTS. The y-axis completes a right-handed system.
- body frame (b): this frame is fixed with respect to the robot. The origin is the center of gravity of the robot. The x-axis is aligned with the forward driving direction. The y-axis forms a right-handed system.

In Figure 2, the x-/y-/z-axis of the coordinate systems are coloured as red/green/blue, respectively. In our system, the IMU is firmly attached to the platform, and its coordinate frame is aligned to the body frame b. Consequently, they have the same orientation and origin. The measurement from the IMU is in the body frame. The lever arms (see Figure 1) between the IMU and the prism are taken from CAD (Computer-Aided Design) model of the robot.

As the measurements are in body frame or RTS frame and the location or the state of the robot should be in the local reference frame, coordinate transformations between the systems are necessary. The lever arms need to be considered. The necessary transformations will be described as follows:

- between the RTS frame and the local reference frame ($t \leftrightarrow l$): as the z-axes of the two coordinate systems are parallel and point toward the same direction, just one rotation (α) and three translations (X_0, Y_0, Z_0) are necessary to transform the RTS frame to the local reference frame. These parameters can be calculated by free stationing using identical points in both coordinate systems.
- between the body frame and the local reference frame ($b \leftrightarrow l$): this is achieved by three translations and three rotations. Three translations are the position $\boldsymbol{p}$ in the state vector, and the three rotations can be calculated by the quaternion $\boldsymbol{q}$, which are estimated in each iteration of the filter.

The equations of the different transformations will not be given in this paper. It needs to be mentioned that one coordinate system is not illustrated in Figure 2, which could be called the robot base footprint frame. This coordinate system is defined by the start position and orientation of the robot and could be considered as the body frame at epoch 0. The relative positions and orientations measured by the odometer are with regard to this start position.

4 EXPERIMENTAL RESULTS AND EVALUATION

4.1 Test Scenario

To evaluate the implemented filter, a test was performed in the Large-Scale Construction Robotics Laboratory (LCRL) of the IntCDC in Stuttgart in June 2024.

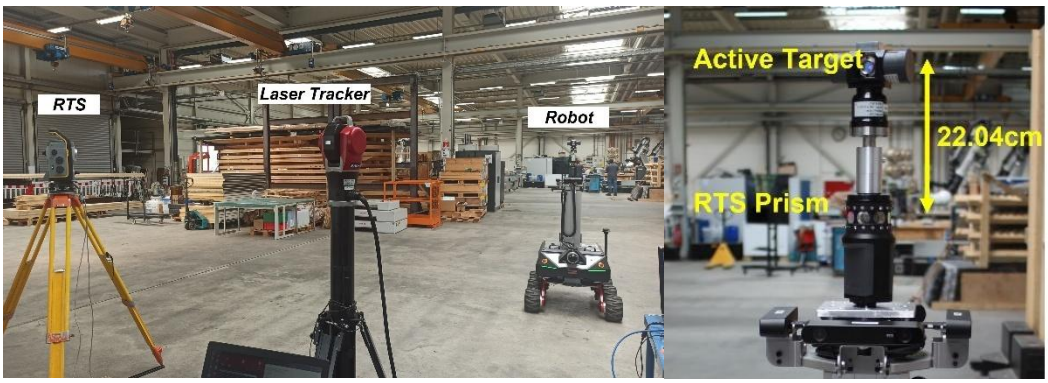

Figure 3: Test Scenario with reference measurement from laser tracker (left) and lever arm between RTS prism and active target (right)

For the evaluation of the accuracy, a ground truth is necessary. A laser tracker API Radian (API Radian, 2022, see Figure 3 left) with a maximum permissible error of ±10µm + 5 ppm was used, which uses its own prism (active target) and is different from that of RTS. In Figure 3 (right), the two prisms and the lever arm between them are shown. The length of the lever arm is 22.04 cm, which was measured by a laser tracker. Five points were measured by the laser tracker and then by RTS. The local reference frame (l) is defined in our case by the laser tracker directly. Free stationing is carried out to calculate the transformation parameter between the local reference frame (l) and the RTS frame (t). The sampling rate of laser tracker is 5 Hz.

During the test, there is always LoS between the prism on the robot and RTS. To evaluate the robustness of the system, some RTS measurements are deleted to simulate that there were no measurements available from RTS due to e.g. the loss of LoS (called RTS “offline”). It means the ES-EKF is running

only with the IMU and odometer data and “drift” in the system can be evaluated, if the RTS measurements were available again (called RTS “online”).

4.2 Results and Discussion

4.2.1 Accuracy Evaluation

The robot ran several circles for about 8 minutes, with an average velocity of 0.35m/s. Figure 4 shows the trajectories of the ES-EKF and those from the laser tracker in 2D (horizontal plane) and 3D. For a better comparison, the ES-EKF was calculated with respect to the RTS prism.

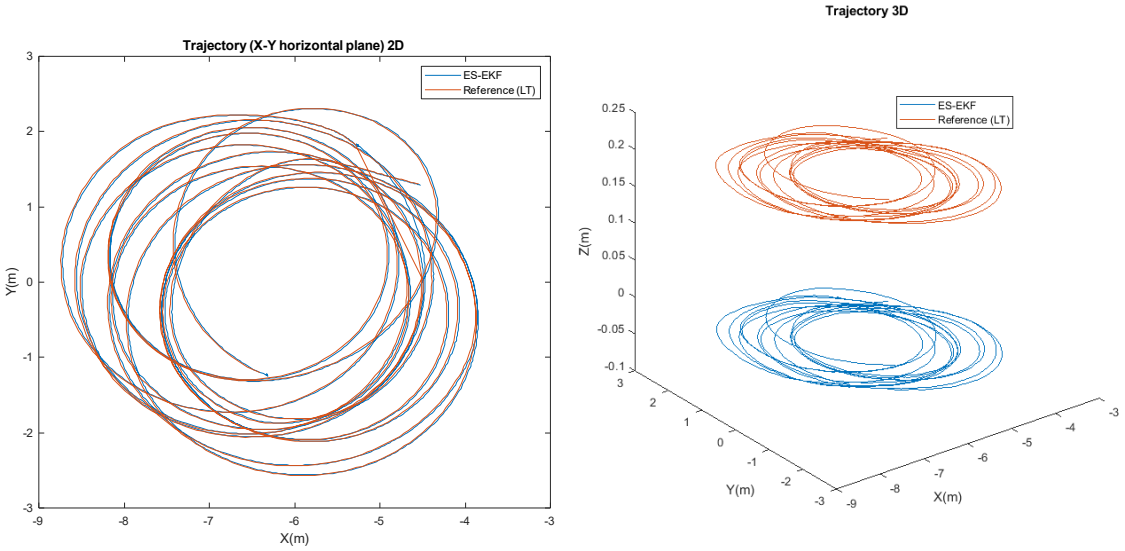

Figure 4: Trajectories Comparison from ES-EKF and Laser Tracker 2D (left) and 3D (right)

It can be seen in Figure 4, that trajectories fit very well to each other in horizontal plane (their difference could almost not be seen in the scale of Figure 4), and height difference are about 20 cm, because, as explained in section 4.1, the ES-EKF results are from the RTS prism and laser tracker measurements are from the active target. The trajectories are from different targets. And the measurement point of time of RTS and laser tracker are different, so direct point-to-point comparison is not possible for consistent evaluation. For this reason, the software SpatialAnalyzer (SA) (SpatialAnalyzer, 2025) was used for a point-to-curve comparison.

Figure 5 illustrates the procedure: a curve, using the laser tracker points, was estimated as a B-Spline by SA. Then the distance (perpendicular to the curve) from ES-EKF points to the curve was estimated. The results show that the maximum and minimum distances are 23.19cm and 20.77cm, respectively. About 87% of the distance is between 22.59cm and 21.98cm and the mean value of the distance is 22.35cm, and the standard deviation is 0.3cm. As the length of the lever arm between the RTS prism and the active target is 22.04cm, the difference between the reference and the mean value is 0.31cm, and considering the standard deviation of 0.3cm, the difference between the reference and the mean value is not significant.

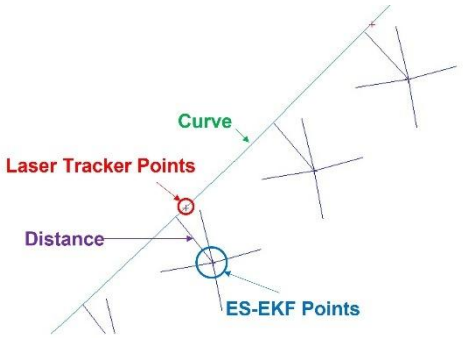

Figure 5: Analysis in SA

4.2.2 Robustness Evaluation

To evaluate the robustness of ES-EKF in case of loss of LoS, 90 seconds of RTS measurements were deleted. The ES-EKF performance after the absence of RTS data can be analysed. It will be shown how it recovers when the RTS measurements are available again (RTS online).

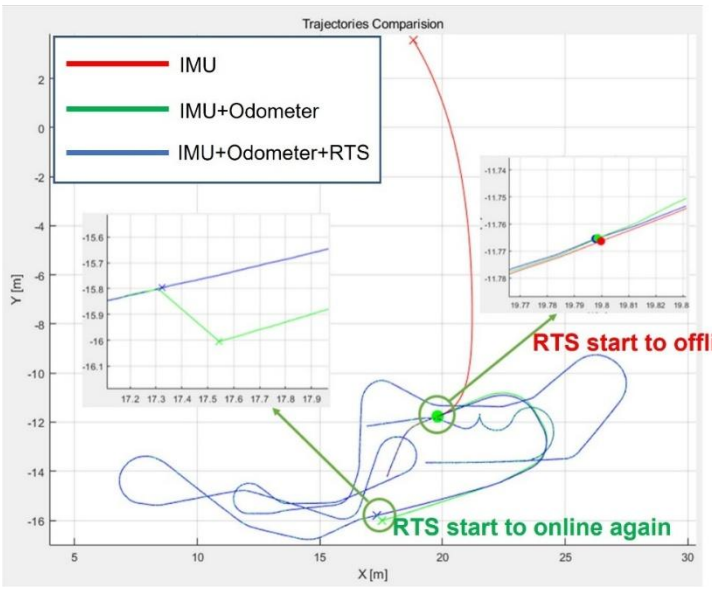

Figure 6: Trajectory comparison for RTS offline Test (Yi ,2024)

In Figure 6, the trajectories of ES-EKF under 3 conditions are represented. The ES-EKF without odometry started to diverge after the unavailability of RTS measurement (RTS offline), while ES-EKF with odometry drifted slowly after the unavailability of RTS measurement and recovered immediately when RTS was online again; it drifted about 0.3m until RTS measurements were available (90 seconds) again. The ES-EKF without RTS and odometer data (it means only the IMU data) drifted about 0.5m after only 5 seconds. The results show that the odometer data is quite reliable and indispensable for the ES-EKF.

5 SUMMARY AND OUTLOOK

In this paper, the methods of integrating the RTS, odometer, and IMU data using the ES-EKF were introduced. The ES-EKF is running in real-time on an indoor robot and could provide precise location or kinematic state (incl. position, velocity, and orientation) of the robot on the construction site. The position difference between the ES-EKF and the laser tracker is only about 0.3cm, and the standard deviation of the difference is 0.3cm, so the difference between ES-EKF and the laser tracker measurement is not significant. In our test, the results of ES-EKF will drift immediately if both the RTS and the odometer data are not available; the result is almost unusable. If only the RTS measurements, e.g., in case of losing the LoS, are not available, the odometer could still be used to correct the drift of the IMU for a short time, depending on the accuracy requirement.

The kinematic state of the robot could be used, in our project, to improve the SLAM result, so that a precise and up-to-date map of the construction site could be generated, which is particularly important in the context of existing buildings. The developed methods could also be used for the localization of the other robots on the construction site, e.g. for the assembly of construction components and so on, if the robots are equipped with RTS prism, IMU, and odometer. The potential of the RTS for positioning on a construction site cannot be underestimated.

REFERENCES

API Radian (2022). RADIAN 3D Laser Tracker Systems. https://topmetrology.ro/wp-content/uploads/2016/09/2019-API-Radian-3D-Laser-Tracker-Systems-Brochure.pdf.

Barbosa, F., Woetzel, J., Mischke, J., Ribeirinho, M.J., Sridhar, M., Parsons, M., Bertram, N., & Brown, S. (2017). Reinventing construction: A route of higher productivity," McKinsey Global Institute, Tech. Rep., 2017.

BMUB (Bundesministerium für Umwelt, Naturschutz, Bau und Reaktorsicherheit) (2017). Reduzierung des Flächenverbrauchs. https://www.bmub.bund.de/WS2220.

Brosque, C., Skeie, G., Örn, J., Jacobson, J., Lau, T., & Fischer, M. (2020). Comparison of Construction Robots and Traditional Methods for Drilling, Drywall, and Layout Tasks. 2020 International Congress on Human-Computer Interaction, Optimization and Robotic Applications (HORA), Ankara, Turkey, 2020. https://doi.org/10.1109/HORA49412.2020.9152871.

Bujanca, M., Shi, X., Spear, M., Zhao, P., Lennox, B., & Luján, M. (2021). Robust SLAM Systems: Are We There Yet? IEEE/RSJ International Conference on Intelligent Robots and Systems (IROS), pp. 5320-5327, 2021. https://doi.org/10.1109/IROS51168.2021.963681

Feng, C., Xiao, Y., Willette, A., Mcgee, W., & Kamat, V. (2014). Towards Autonomous Robotic In-Situ Assembly on Unstructured Construction Sites Using Monocular Vision. https://doi.org/10.13140/2.1.4746.5605.

Gassel, v. F., Schrijver, P.& Lichtenberg, J (2006). Assembling wall panels with robotic technologies, The 23rd ISARC, International Symposium on Automation and Robotics in Construction 2006, Tokyo, October 3 to 5, 2006. https://doi.org/10.22260/ISARC2006/0135.

Guo, A., Zhou, Z., Zhu, X., & Bai, F. (2019). Low-cost sensors state estimation algorithm for a small hand-launched solar-powered UAV. Sensors, vol. 19, p. 4627, Oct. 2019. https://doi.org/10.3390/s19214627

Huang, J., Junginger, S., Liu, H., & Thurow, K. (2023). Indoor Positioning Systems of Mobile Robots: A Review. Robotics 2023, 12, 47. https://doi.org/10.3390/robotics12020047

Lauer, A. P. R., Benner, E., Stark, T., Klassen, S., Abolhasani, S., Schroth, L., Gienger, A., Wagner, H. J., Schwieger, V., Menges, A., & Sawodny, O. (2023). Automated on-site assembly of timber buildings on the example of a biomimetic shell. Automation in Construction, 156, 105118. https://doi.org/10.1016/j.autcon.2023.105118

Liu, W., Song, D., Wang, Z., & Fang, K. (2019). Comparative analysis between error-state and full-state error estimation for KF-based IMU/GNSS integration against IMU faults. Sensors, vol. 19, p. 4912, Nov. 2019. https://doi.org/10.3390/s19224912

IFO (2021). Institute for Economic Research: Shortage of skilled workers on German construction sites worsens. https://www.ifo.de/en/node/65484, last access: 15.08.2025

IntCDC (2018). New Cluster of Excellence: Integrative Computational Design and Construction for Architecture. Proposal for a Cluster of Excellence. Unpublished

Katara, S. (2022). Replenishing the Construction Labor Shortfall. https://www.forbes.com/sites/forbestechcouncil/2022/08/18/replenishing-the-construction-labor. Last access: 15.08.2025

Knippers, J., Kropp, C., Menges, A., Sawodny, O., & Weiskopf, D. (2021). Integratives computerbasiertes Planen und Bauen: Architektur digital neu denken. Bautechnik, vol. 98, no. 3, pp. 194–207, 2021

Madyastha, V., Ravindra, V., Mallikarjunan, S., & Goyal, A. (2011). Extended Kalman Filter vs. Error State Kalman Filter for aircraft attitude estimation," in AIAA Guidance, Navigation, and Control Conference, American Institute of Aeronautics and Astronautics, June 2011. https://doi.org/10.2514/6.2011-6615

Markovic, L., Kovac, M., Milijas, R., Car, M., & Bogdan, S. (2022). Error State Extended Kalman Filter Multi-Sensor Fusion for Unmanned Aerial Vehicle Localization in GPS and Magnetometer Denied Indoor Environments. 2022 International Conference on Unmanned Aircraft Systems (ICUAS), 184-190. https://doi.org/10.1109/ICUAS54217.2022.9836124

Maybeck, P. S. (1979). Stochastic models, estimation, and control. Volume 1, Academic Press, New York, 1979.

Meyer, H. J. (2003). Anwendung von geodätischen Positionsmesssystemen in Straßenbaumaschinen. Baumaschinentechnik 2003 – Erfahrungen, Methoden, Innovationen – Fachtagung 20./21.03.2003 Dresden. Heft Nr. 23 der Schriftenreihe der Forschungsvereinigung Bau- und Baustoffmaschinen

Shohet, I. M., & Rosenfeld, Y (1997). Robotic mapping of building interior—precision analysis. Automation in construction, 7(1):1-12, 1997. https://doi.org/10.1016/S0926-5805(97)00030-7

Sola, J. (2017): Quaternion kinematics for the error-state Kalman filter. arXiv preprintarXiv:1711.02508.

Sorour, M.T., Abdellatif, M. A., Ramadan, A.A., & Abo-Ismail, A. A. (2011). Development of roller-based interior wall painting robot. World Academy of Science, Engineering and Technology 59.

SpatialAnalyzer (2025). Software SpatialAnalyzer. https://www.kinematics.com/.

Tichelmann, K.U., Blome, D., Günther, M., & Groß, K. (2016). Deutschland Studie 2015. Wohnraumpotentiale durch Aufstockungen, TU Darmstadt, Darmstadt. https://www.twe.architektur.tu-darmstadt.de/media/twe/publikationen_13/Deutschlandstudie2015_ohne_best_practice_beispiele.pdf.

Vähä, P., Heikkilä, T., Kilpeläinen, P., Jarviluoma, M. & Gambao, E. (2013). Extending automation of building construction — Survey on potential sensor technologies and robotic applications. Automation in Construction. 36. 168–178. https://doi.org/10.1016/j.autcon.2013.08.002.

Vectorav (2025). Data Sheet of VN-100 IMU/AHRS. https://www.vectornav.com/resources/detail/vn-100-product-brief

Warszawski, A., & Navon, R. (1986). Development of a Robot for Interior Finishing Works. 4th International Symposium on Automation and Robotics in Construction. https://doi.org/10.22260/ISARC1987/0015.

Yi, Q. (2024). Development and evaluation of a real-time error state Kalman Filter for localization of an indoor robot. Master Thesis at Institute of Engineering Geodesy and Visualization Research Center at the University of Stuttgart.

Youn, W., & Gadsden, S. A. (2019). Combined quaternion-based error state Kalman filtering and smooth variable structure filtering for robust attitude estimation," IEEE Access, vol. 7, pp. 148989–149004, 2019. https://doi.org/10.1109/ACCESS.2019.2946609

ACKNOWLEDGEMENTS

This contribution is supported by the Deutsche Forschungsgemeinschaft (DFG, German Research Foundation) under Germany's Excellence Strategy – EXC 2120/1 – 390831618. The authors cordially thank the funding agency.

BIOGRAPHICAL NOTES

M.Sc. **Sahar Abolhasani**

2004 – 2008 Studies of Survey in Iran (Shahid Rajaee University)
2009 – 2012 Studies of Survey and Geodesy in Iran (Tehran University)
2012-2013 Teacher at the chair of Geodesy in Iran (University of Qom)
2013-2021 Geodesy Engineer in Iran (Saman Sad Roud Consulting Engineering)
Since 2021 Research Associate at Institute of Engineering Geodesy (University of Stuttgart)

Dr.-Ing. **Li Zhang**
2002 – 2003 Studies of Remote Sensing and Geoinformation in China (University of Wuhan)
2004 – 2009 Studies of Geodesy and Geoinformation in Germany (University of Stuttgart)
Since 2009 Research Associate at Institute of Engineering Geodesy (University of Stuttgart)
2016 Dr.-Ing. Geodesy (University of Stuttgart)
2015 – 2018 Vice Chair Administration of FIG Commission 5 "Positioning and Measurement"
Since 2019 Co-Chair of FIG Commission 5- WG5.6 "Cost Effective Positioning"
Since 2019 Chair of Working Group "Quality Assurance of Measurement Data" in Commission 3 "Measurement Methods and Systems" of DVW (German Association of Surveying)

Prof. Dr.-Ing. habil. Dr. h.c. **Volker Schwieger**
1983 – 1989 Studies of Geodesy in Hannover
1989 Dipl.-Ing. Geodesy (University of Hannover)
1998 Dr.-Ing. Geodesy (University of Hannover)
2004 Habilitation (University of Stuttgart)
since 2010 Professor and Head of Institute of Engineering Geodesy, University of Stuttgart
2015 – 2018 Chair of FIG Commission 5 ‘Positioning and Measurement’
2016 – 2021 Dean of the Faculty of Aerospace Engineering and Geodesy, University of Stuttgart
2019 Dr. h.c., Technical University of Civil Engineering, Bucharest, Romania
2022 Honorary Member of FIG

CONTACTS

M.Sc. Sahar Abolhasani/Dr.-Ing. Li Zhang / Prof. Dr.-Ing. habil. Dr. h.c. Volker Schwieger
University of Stuttgart
Institute of Engineering Geodesy
Geschwister-Scholl-Str. 24 D
D-70174 Stuttgart
GERMANY
Tel. + 49/711685-84054 |-84049 | -84040
Fax + 49/711685-84044
Email: sahar.abolhasani@iigs.uni-stuttgart.de|li.zhang@iigs.uni-stuttgart.de | volker.schwieger@iigs.uni-stuttgart.de
Website: https://www.iigs.uni-stuttgart.de/